

CORRELATION ANALYSIS OF SFI PECULIAR VELOCITIES

STEFANO BORGANI

INFN, Sezione di Trieste, c/o Dipartimento di Astronomia dell'Università, via Tiepolo 11, I-34100 Trieste, Italy
INFN, Sezione di Perugia, c/o Dipartimento di Fisica dell'Università, via A. Pascoli, I-06123 Perugia, Italy

Electronic mail: borgani@ts.astro.it

LUIZ N. DA COSTA

European Southern Observatory, Karl Schwarzschild Str. 2, D-85748 Garching b. München, Germany
Observatório Nacional, Rua Gen. J. Cristino 77, São Cristóvão, Rio de Janeiro, Brazil

Electronic mail: ldacosta@eso.org

IDIT ZEHAVI

NASA/Fermilab Astrophysics Group, Fermi National Accelerator Laboratory,
Box 500, Batavia, IL 60510-0500, U.S.A.

Electronic mail: iditz@simone.fnal.gov

RICCARDO GIOVANELLI AND MARTHA P. HAYNES

Center for Radiophysics and Space Research and National Astronomy and Ionosphere Center¹,
Cornell University, Ithaca, NY 14953

Electronic mail: riccardo@astrosun.tn.cornell.edu, haynes@astrosun.tn.cornell.edu

WOLFRAM FREUDLING

Space Telescope–European Coordinating Facility, European Southern Observatory,
Karl Schwarzschild Str. 2, D-85748 Garching b. München, Germany

Electronic mail: wfreudli@eso.org

GARY WEGNER

Department of Physics and Astronomy, Dartmouth College, Hanover, NH 03755, U.S.A.//Electronic mail:

wegner@kayz.dartmouth.edu

JOHN J. SALZER

Department of Astronomy, Wesleyan University, Middletown, CT 06459, U.S.A.

Electronic mail: slaz@parcha.astro.wesleyan.edu

ABSTRACT

We present results of a statistical analysis of the SFI catalog of peculiar velocities, a recently completed survey of spiral field galaxies with I-band Tully-Fisher distances. The velocity field statistic utilized is the velocity correlation function, $\psi_1(r)$, originally introduced by Górski et al. (1989). The analysis is performed in redshift space, so as to circumvent potential ambiguities connected with inhomogeneous Malmquist bias corrections. The results from the SFI sample are compared with linear-theory predictions for a class of cosmological models. We generate a large set of mock samples, extracted from N-body simulations, which are used to assess the reliability of our analysis and to estimate the associated uncertainties. We assume a class of CDM-like power spectrum models, specified by σ_8 , the r.m.s. fluctuation amplitude within a sphere of $8h^{-1}$ Mpc radius, and by the shape parameter Γ . Defining $\eta_8 = \sigma_8 \Omega_0^{0.6}$, we find that the measured $\psi_1(r)$ implies a degenerate constraint in the η_8 - Γ plane, with $\eta_8 = 0.3 \pm 0.1(\Gamma/0.2)^{0.5}$, at the 2σ level, for the inverse Tully-Fisher (ITF) calibration presented in this paper. We investigate by how much this constraint changes as we account for uncertainties in the analysis method and uncertainties in the distance indicator, and consider alternative ITF calibrations. We find that both changing the error weighting scheme and selecting galaxies according to different limiting line-widths has a negligible effect. On the contrary, the model constraints are quite sensitive to the ITF calibration. The other ITF calibrations by Giovanelli et al. (1997) and da Costa et al. (1998) both give, for $\Gamma = 0.2$, $\eta_8 \simeq 0.6$ as the best-fitting value. FERMILAB-Pub-99/133-A

¹The National Astronomy and Ionosphere Center is operated by Cornell University under a cooperative agreement with the National Science Foundation.

1 INTRODUCTION

The peculiar velocity field of galaxies provides a very powerful way of probing mass fluctuations on intermediate to large scales ($\lesssim 100 h^{-1}$ Mpc, h being the Hubble constant in units of $100 \text{ km s}^{-1} \text{ Mpc}^{-1}$), as it is sensitive primarily to large scale density fluctuations. Therefore, studies of cosmic flows can be used to constrain the amplitude of the large-scale mass power-spectrum, thus complementing the information on intermediate scales, between those probed by redshift surveys and those sampled by anisotropies in the cosmic microwave background (CMB) as observed by COBE (see the review by Dekel 1994). Another advantage in studying the velocity field is that it is measured on scales where linear approximation to gravitational instability is expected to hold, thus allowing one to explore more thoroughly the parameter space of cosmological models. We can parameterize the fluctuation power spectrum in terms of the r.m.s. fluctuation within spheres of $8h^{-1}\text{Mpc}$, σ_8 , and of a shape parameter Γ . Then, according to linear theory, the typical amplitude of the peculiar velocity on a given scale is proportional to $\eta_8 f(\Gamma, R)$, where $\eta_8 = \sigma_8 \Omega_m^{0.6}$ (following the notation of Chiu, Ostriker & Strauss 1998; Ω_m here is the matter density parameter) and $f(\Gamma, R)$ is a quantity which depends on the power spectrum shape and on the scale R at which the velocity field is probed.

Several statistical characterizations of the peculiar velocity fields have been proposed in the last decade, with the aim of providing more robust constraints on cosmological scenarios, as newer and larger data sets came to completion (e.g., Strauss & Willick 1995, for a review). Among such statistical measures, in this paper we will concentrate on the velocity correlation function, which has been introduced for turbulence studies by Monin & Yaglom (1975) and borrowed for cosmology by Peebles (1980; cf. also Górski 1988). We will apply this statistic to the SFI sample, a recently completed homogeneous all-sky survey of Sbc-Sc galaxies with I-band Tully-Fisher (TF) distances (Giovanelli et al. 1997a; Haynes et al. 1999a,b, H99a,b).

A first application of the velocity correlation statistics to observational data was realized by Górski et al. (1989, G89 hereafter; see also Groth, Juskiewicz & Ostriker 1989), who analyzed the spiral galaxy sample by Aaronson, Huchra & Mould (1979) and the elliptical galaxy sample by Burstein et al. (1987), finding substantial discrepancies between the results obtained from these two data sets. Tormen et al. (1993, T93) analyzed the correlation statistics of the Mark II sample, with results favoring $\eta_8 \simeq 0.7$ for scale-invariant CDM models. Kolatt & Dekel (1996) estimated the matter power-spectrum implied by the POTENT reconstruction of the Mark III data (Willick et al. 1997) and found $\eta_8 \simeq 0.7-0.8$. More recently, maximum-likelihood analyses, estimating the mass power-spectrum that gives rise to the observed peculiar

velocities, have been performed by Zaroubi et al. (1997) on the Mark III sample and by Freudling et al. (1999, FZ99) on the SFI sample. Both analyses consistently find $\eta_8 \simeq 0.8 \pm 0.2$ (90% c.l.), quite independent of the power-spectrum shape. These results point toward high-amplitude fluctuations, thus somewhat at variance with results from the r.m.s. cluster peculiar velocity (e.g., Borgani et al. 1997; Watkins 1997) and with constraints from the local cluster abundance (e.g., Eke, Cole & Frenk 1996; Girardi et al. 1998), which indicate lower values.

Studies of the peculiar velocity can also be combined with analyses of all-sky redshift surveys to investigate the relation between the galaxy and underlying mass distributions, a key ingredient for understanding galaxy biasing. Comparisons between the measured peculiar velocities or the recovered densities with those predicted from all-sky redshift surveys are commonly used to estimate the parameter $\beta = \Omega_m^{0.6}/b$, under the assumption of linear biasing with a bias factor b . Several estimates of β have been presented in the literature (e.g., da Costa et al. 1998; Willick & Strauss 1998; Branchini et al. 1999, and references therein) based on comparisons between the velocity fields directly inferred from TF data and recovered from galaxy density field in the IRAS 1.2 Jy (Fisher et al. 1995) and PSCz survey. Such analyses generally find β values in the range 0.5–0.7. Taking $b = \sigma_{8,IRAS}/\sigma_8$, these results would imply $\eta_8 \simeq 0.35-0.50$ for $\sigma_{8,IRAS} \simeq 0.7$ (Fisher et al. 1994). On the other hand, analyses based on the comparison of density fields provide values of β as large as 0.9 (e.g., Sigad et al. 1998). The interpretation of the β values is further complicated if galaxy biasing is better described by a stochastic, nonlinear process (e.g., Dekel & Lahav 1999).

The aim of this paper is to perform a detailed analysis of the velocity correlation function for the SFI sample and to derive the resulting constraints on large-scale structure formation models. The comparison to theoretical expectations is based on linear-theory predictions and we resort to large-scale N-body simulations to verify the reliability of our analysis and to estimate the associated errors, contributed by both the cosmic variance and by the scatter in the TF relation.

In our analysis, we choose to use redshift-space information as the indicator of distance for the SFI galaxies, so as to avoid the associated Malmquist bias arising from the intrinsic scatter of the distance indicator when using the inferred distances (cf. Freudling et al. 1995, for a discussion on bias corrections in the SFI sample). The forward TF relation, obtained by regressing the apparent magnitudes over the line-width, in this case, is still susceptible to selection bias due to the imposed magnitude-limit. Using the inverse relation, i.e. fitting the line-width as a function of the apparent magnitude, avoids this selection bias, as long as the sample selection is independent of the

line-width (see §6 of Strauss & Willick 1995, and references therein). For this reason, we perform our analysis in redshift-space by using peculiar velocities estimated from the inverse Tully-Fisher (ITF) relation.

The outline of the paper is as follows. In Section 2 we provide a basic description of the SFI sample and present the ITF calibrations on which our analysis is based. Section 3 contains a brief introduction to the velocity correlation formalism and presents the results of its application to the SFI data. In Section 4 we present the velocity correlation analysis of our mock samples. In Section 5 we derive the resulting constraints on cosmological models and discuss the impact of systematic effects in both the sample definition and the correlation analysis method. We summarize our main conclusions in Section 6.

2 THE SFI SAMPLE

The TF data defining the sample used here consists of two main datasets: a subset of the Mathewson, Ford & Buchhorn (1992) survey with about 1200 galaxies with I-band photometry and measured rotational velocities, either from radio observations of 21-cm line-widths or optical rotation curves; the SFI I-band TF redshift-distance survey of about 1300 Sbc-Sc field galaxies. The SFI sample consists of galaxies with inclination $\gtrsim 45^\circ$ north of $\delta < -45^\circ$ and galactic latitudes $|b| > 10^\circ$. The original Mathewson et al. (1992) measurements of magnitude and rotational velocities were converted into the SFI system using about 200 to 300 common galaxies.

In addition to the field galaxies, roughly 800 galaxies covering a broader range of morphological types were observed in the field of 24 clusters (Giovanelli et al. 1997a,b; SCI sample). After careful membership assignment, cluster galaxies were used to derive a combined TF relation corrected for Malmquist bias and bias introduced by incompleteness and different morphological mix. In order to perform our analysis in redshift-space, we consider the inverse TF relation (ITF, hereafter) between the absolute magnitude M and the full line-width W ,

$$M = a + b(\log W - 2.5), \quad (1)$$

with $a = -20.95$ and $b = -7.94$ (here W is expressed in units of km s^{-1} and we assume a Hubble constant of $100 \text{ km s}^{-1} \text{ Mpc}^{-1}$). This relation has the same slope as that originally provided by Giovanelli et al. (1997b, G97 hereafter), whose zero-point, $a = -21.10$, is 0.15 magnitudes smaller. This difference is due to a new determination of the velocity widths and to the removal of 71 galaxies due to poor photometry, poor line-widths or obvious misidentification (cf. H99a,b). The 1σ uncertainty in the zero-point has been estimated by G97 to be about 0.05 magnitudes, when combining statistical uncertainties

in the TF fitting and uncertainties in defining the cluster reference frame with a finite number (24) of such objects. This uncertainty does not however include possible systematics associated with the processing of the raw data or with difference between the TF relation of clusters and field galaxies, or potential deviations of our local universe from a global Hubble flow (e.g. Zehavi et al. 1998, but see also Giovanelli et al. 1999).

We note that careful analysis of the TF relation for galaxies in clusters suggests that the scatter depends on the line-width. This dependence is modeled by letting the error in the estimated distance r_i of the i -th galaxy to be $\epsilon_i = \Delta(W_i)r_i$, where $\Delta(W_i)$ is the fractional error in the distance as estimated from the scatter about the ITF relation as a function of the measured line-width of the galaxy (G97, cf. also Willick et al. 1997 and Willick & Strauss 1998). The resulting errors are estimated to be in the range 15–20%.

Unless otherwise specified and following da Costa et al. (1996) and FZ99, we discard those ($\sim 7\%$) SFI galaxies with line-width $\log W \leq 2.25$, because of the limited reliability of the ITF relation at such line-widths. We will also show the robustness of the final results against changes in the assumed limiting line-width. Furthermore, we restrict our analysis to the SFI subsample defined by galaxies lying within $cz \leq 6000 \text{ km s}^{-1}$. With such restrictions, the final sample on which we base our analysis contains 974 galaxies.

A further alternative calibration of the ITF has been presented by da Costa et al. (1998, dC98 hereafter), based on a comparison of the velocity field of the SFI sample and that implied by the IRAS 1.2 Jy survey. The resulting zero-point and slope of the ITF are $a = -21.11$ and $b = -8.55$, respectively. In the following, we will use the above most recent ITF calibration as the reference one, but will show the effect of taking the previous G97 and dC98 calibrations on the final constraints on cosmological parameters.

3 THE VELOCITY CORRELATION STATISTICS

The estimator for the velocity correlations that we will use in the following is that introduced by G89 and is given by

$$\psi_1(r) = \frac{\sum_{|\mathbf{r}_i - \mathbf{r}_j| = r} w_i w_j u_i u_j \cos \vartheta_{ij}}{\sum_{|\mathbf{r}_i - \mathbf{r}_j| = r} w_i w_j \cos^2 \vartheta_{ij}}, \quad (2)$$

where ϑ_{ij} is the angle between the direction of the i -th and the j -th galaxy and the sums are over all the galaxy pairs at separation r in redshift space. With the above definition, the $\Psi_1(r)$ statistics is independent of any assump-

tions regarding the velocity field, such as homogeneity and isotropy, and has been shown by G89 to be rather robust to sampling fluctuations. In eq.(2) u_i is the radial peculiar velocity of the i -th galaxy and w_i represents a suitable weight to be assigned to it. The introduction of the weights is a slight modification of the expression for ψ_1 provided by G89 (see also T93). Different weighting schemes will be applied in the following: (1) uniform weighting, $w_i = 1$; (2) weighting galaxies according to their distance-error, $w_i = 1/\epsilon_i$; (3) weighting according to $w_i^2 = 1/(\epsilon_i^2 + \sigma_f^2)$, where σ_f^2 is the variance of the local velocity field.

The quantity σ_f can be interpreted as a line-of-sight velocity dispersion and has been introduced in order to model possible non-linearities, which generates small-scale random motions within virialized regions. Such motions, which would give rise to an uncorrelated velocity component, are expected to be relatively unimportant for the SFI field galaxies, whose peculiar velocity should not be much affected by virial motions. A further possible interpretation of σ_f is an unrecognized distance-independent error, which is not accounted for by the ITF scatter calibrated by using members of distant clusters (e.g., Kaiser 1988). FZ99 checked for such a term by having it as a further degree of freedom to be constrained by a maximum likelihood approach and found $\sigma_f = 200 \pm 120 \text{ km s}^{-1}$. When resorting to the weighting scheme (3), we will take $\sigma_f = 150 \text{ km s}^{-1}$, although our final results are essentially insensitive to its choice.

As for the scheme (1), its main drawback is that it assigns the same weight to all objects, regardless of the uncertainty in the velocity errors, which increase with distance. Although the methods (2) and (3) overcome this limitation, they reduce the effective sampling volume, and have been shown by Dekel, Bertschinger & Faber (1990) to overestimate the contribution of well sampled regions with respect to under-sampled regions in the reconstruction of velocity fields. In the following we will mainly base our analysis on the uniform-weighting scheme, which is the least affected by cosmic scatter (see Section 4 below).

As shown by G89, the ensemble average of $\psi_1(r)$ is given by

$$\Psi_1(r) = \langle \psi_1(r) \rangle = \mathcal{A}(r)\Psi_{\parallel}(r) + [1 - \mathcal{A}(r)]\Psi_{\perp}(r), \quad (3)$$

under the assumption of homogeneity and isotropy, where Ψ_{\parallel} and Ψ_{\perp} are the radial and transverse correlation functions of the three-dimensional peculiar velocity field. In linear theory, they are connected to the power-spectrum of density fluctuations, $P(k)$, according to

$$\begin{aligned} \Psi_{\parallel}(r) &= \frac{f(\Omega_m)^2 H_0^2}{2\pi^2} \int dk P(k) \left[j_0(kr) - 2\frac{j_1(kr)}{kr} \right]; \\ \Psi_{\perp}(r) &= \frac{f(\Omega_m)^2 H_0^2}{2\pi^2} \int dk P(k) \frac{j_1(kr)}{kr}, \end{aligned} \quad (4)$$

where $j_i(x)$ is the i -th order spherical Bessel function and

$$f(\Omega_m) \simeq \Omega_m^{0.6}.$$

The quantity \mathcal{A} appearing in eq.(3) is a moment of the selection function of the sample depending on the spatial distribution of galaxies according to

$$\mathcal{A}(r) = \frac{\sum_{|\mathbf{r}_i - \mathbf{r}_j| = r} w_i w_j [r_i r_j (\cos \vartheta_{ij} - 1) + r^2 \cos \vartheta_{ij}] \cos \vartheta_{ij}}{r^2 \sum_{|\mathbf{r}_i - \mathbf{r}_j| = r} w_i w_j \cos^2 \vartheta_{ij}} \quad (5)$$

This quantity provides in a sense the relative contribution to $\psi_1(r)$ from the radial and transverse components of the velocity correlation. The definition of eq.(5) is slightly different from that previously adopted by other authors, by including the galaxy weights.

The advantage of using ψ_1 is that it can directly be calculated from the observed radial velocities, without the need of any additional assumption. It can then be related to theory (eq.[3],[4]), taking into account the specific sampling through eq.(5). The geometrical factor $\mathcal{A}(r)$ is plotted in Figure 1 for the three mentioned weighting schemes. The net effect of a non-uniform weighting is that of increasing $\mathcal{A}(r)$ at separations $\gtrsim 2000 \text{ km s}^{-1}$. This is the consequence of the fact that Ψ_{\perp} takes relatively more contribution than Ψ_{\parallel} from large-scale fluctuations (see, e.g., Gorski 1988). Therefore, its contribution to $\Psi_1(r)$ is suppressed with the error weighting, which amounts to decreasing the effective volume of the sample.

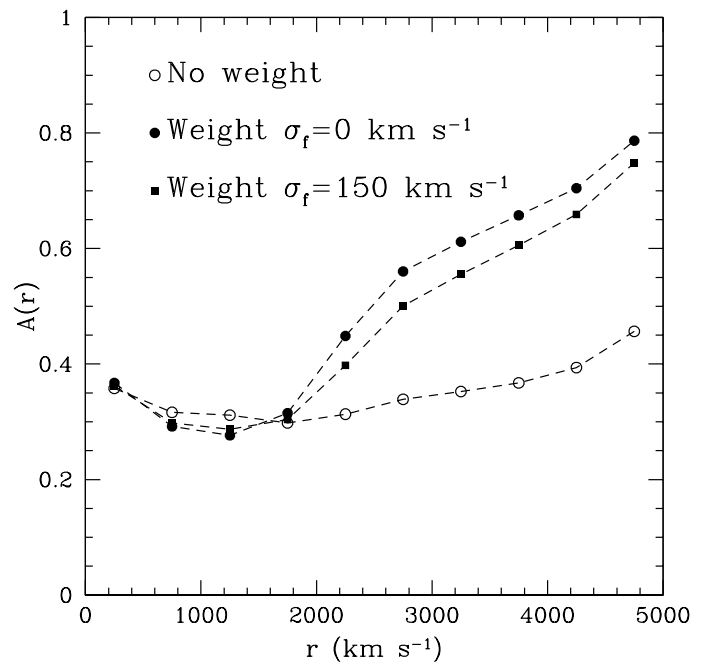


Fig. 1.— The geometrical factor $\mathcal{A}(r)$ (eq.[5]; see text), associated with the SFI sample, for the three alternative weighting schemes.

The velocity correlation function $\psi_1(r)$ for the SFI sample, with the H99 calibration, computed within bins of 500 km s^{-1} , is plotted in Figure 2. No errorbars are assigned here to $\psi_1(r)$. We will discuss in the next section how to associate uncertainties to model predictions, in order to provide confidence levels in the estimate of cosmological parameters. The upper panel shows the effect of adopting different weighting schemes. It is apparent that the choice for w_i has a marginal impact on the correlation signal. This result might seem somewhat unexpected, in view of the different $A(r)$ values for the weighted and unweighted cases. However, these differences appear only at rather large separations, $r \gtrsim 2000 \text{ km s}^{-1}$ (cf. Figure 1), where the value of ψ_1 for SFI rapidly declines, thus making any difference among different weighting schemes hardly detectable. By comparing this result with that from the real-space analysis of the Mark II sample by Tormen et al. (1993), it turns out that the SFI sample produces a velocity correlation signal which is at least a factor two smaller, although the corresponding scales at which $\psi_1(r)$ approaches zero ($\simeq 3000 \text{ km s}^{-1}$) are similar.

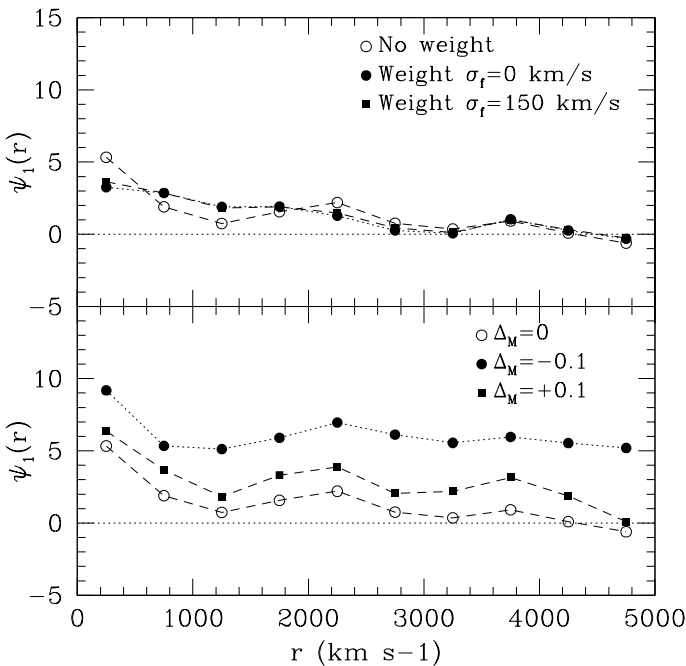


Fig. 2.— The velocity correlation function, $\psi_1(r)$ (in units of 10^4 km s^{-1}), for the SFI sample. The upper panel shows the effect of different galaxy weights, while the lower panel shows the effect of changing by 0.1 magnitudes the zero-point of the ITF relation, representing the 2σ uncertainty in its calibration (cf. G97, H99a,b).

The lower panel of Fig. 2 shows the effect of changing the zero-point of the ITF relation (eq.[1]) by 0.1 magnitudes either way, which corresponds to a change of $\epsilon \sim 2.5\%$ in the distances or an additional global

Hubble-like flow ϵr . This change corresponds to the 2σ formal statistical uncertainty estimated from the analysis of the SCI sample of cluster galaxies (G97, H99a,b). A global Hubble-like flow represents a coherent velocity field which is characterized by a positive correlation (i.e., galaxies moving in the same direction) on intermediate scales, $r \lesssim 5000 \text{ km s}^{-1}$ and by a negative correlation at the largest scales, $r \gtrsim 7000 \text{ km s}^{-1}$, when the two galaxies of a pair are placed in the opposite directions of the sample.

Alternative estimators of the velocity correlation statistics have been applied by different authors. Groth et al. (1989; cf. also Kaiser 1988) considered the generic form for the velocity correlation tensor under the assumption of homogeneous and isotropic velocity field, $\Psi_{ij}(r) = \langle v_i(\vec{x})v_j(\vec{x} - \vec{r}) \rangle = \Psi_{\perp}(r)\delta_{ij} + [\Psi_{\parallel}(r) - \Psi_{\perp}(r)]\hat{r}_i\hat{r}_j$, where δ_{ij} is the Kronecker symbol. Then, they obtained Ψ_{\perp} and Ψ_{\parallel} by a χ^2 -minimization procedure to the data. G89 compared this method to their $\Psi_1(r)$ approach and showed that they produce comparable results, although the former turns out to be noisier at large separations, $r \gtrsim 4000 \text{ km s}^{-1}$.

More recently, Ferreira et al. (1999) proposed a new method to estimate the main galaxy pairwise velocity, $\vec{v}_{12} = \langle \vec{v}(\vec{x}_1) - \vec{v}(\vec{x}_2) \rangle$. This method, which has been so far tested on N-body mock samples and is in the process of being applied to real data sets, provides essentially constraints on $\sigma_8^2\Omega_m^{0.6}$. Therefore, its combination with linear-theory constraints on $\sigma_8\Omega_m^{0.6}$ could in principle break the degeneracy between σ_8 and Ω_m . Of course, careful investigations are required in order to understand whether available data are of sufficient quality and their systematics and biases are enough under control to allow a reliable estimate of σ_8 and Ω_m separately.

4 ANALYSIS OF THE MOCK SAMPLES

In order to explore extensively the model parameter space, we resort in the following to linear theory as the means to compare model predictions and SFI results. Two important issues need to be addressed: (a) the reliability of our analysis and specifically the use of linear theory to predict the statistics of the velocity field, and (b) the estimate of the cosmic scatter and the observational uncertainties associated with the SFI sampling, in order to establish the confidence level for model exclusion. For this purpose we use large N-body simulations from which we extract sets of mock samples which mimic the sampling and selection effects of the SFI sample.

4.1 Generating the mock samples

The parent N-body simulations from which we extract mock samples have been run by using the publicly available adaptive P^3M code by Couchman (1991). We have run two simulations corresponding to two different cosmological scenarios. The first model is a flat low-density one with $\Omega_m = 0.4$ ($\Lambda 0.4$). The transfer function used is that of Bardeen et al. (1986) [see eq.(7) below], with the shape parameter Γ set to 0.22 and $\sigma_8 = 0.87$. The second model is an Einstein–de Sitter (EdS) universe, with $\Gamma = 0.43$, and $\sigma_8 = 1.2$. With the above parameters, both models are consistent with the 4-year *COBE* normalization (e.g., Bunn & White 1997), while the EdS model fails to match the abundance of local galaxy clusters (e.g., Eke et al. 1996; Girardi et al. 1998) and the shape of the galaxy power-spectrum (e.g., Peacock & Dodds 1994; Liddle et al. 1996).

Each simulation follows 128^3 particles within a box of $250h^{-1}\text{Mpc}$ on a side. The adopted Plummer softening scale, $\simeq 100h^{-1}\text{kpc}$, is more than adequate to describe the large-scale velocity field (see Borgani et al. 1999, for a more detailed description of the simulations). Velocity fields on scales of a few $\times 10h^{-1}\text{Mpc}$, which are of interest in this paper, receive a small but non-negligible contribution from wavelengths larger than the adopted box size. Furthermore, the volume of a single simulation can accommodate only a rather small number of non-overlapping SFI mock samples (each extending out to $cz = 6000\text{ km s}^{-1}$), so as to not allow a reliable determination of cosmic variance.

In order to extend the dynamic range of our simulations to larger scales, we resorted to the method proposed by Tormen & Bertschinger (1996) of adding longer waves to N-body outputs. This method, which allows to generate non-periodic replicas of a parent box, is based on the Zel’dovich approximation (Zel’dovich 1970) for computing the contribution to particle displacements and velocities from waves longer than the original box size. Cole (1997) showed that this procedure is adequate to extend to larger scales the description of peculiar velocities. In our analysis, we replicate the original box three times along each spatial direction, which leads to a total of 27 replica and a final box of size $L = 750h^{-1}\text{Mpc}$, containing about 5.7×10^7 particles.

As a first step for mock sample extraction, we divide the large box into 6^3 smaller boxes of $125h^{-1}\text{Mpc}$ on a side. At the center of each of them we place an observer. After randomly choosing the orientation of the “galactic” coordinate system, we select among the simulation particles those which are closest to the position of real galaxies in the SFI sample. In this way, we generate mock samples with the same spatial distribution and number of galaxies as in the real SFI sample. The “true”

radial velocities in the mock samples are perturbed according to the associated observational errors of the real catalog and according to the assumed random velocity dispersion σ_f (under the assumption that both contributions are independent Gaussian variables). For each simulation, we generate two sets of mock samples, based on assuming both $\sigma_f = 0$ and 150 km s^{-1} . Since the final results turn out to be essentially indistinguishable, we will present for the mock sample analysis only results based on assuming a vanishing σ_f .

We note that other authors (e.g., G89; Strauss, Cen & Ostriker 1993; T93) followed more sophisticated procedures to search for “observers” within simulations. Such procedures involve selecting observers so that local properties of the density and velocity field resemble those observed for the Local Group of galaxies. However, T93 showed that applying such constraints on the observer selection does not significantly alter the velocity correlation statistics for realistic power spectra. Furthermore, the aim of our analysis is to estimate how often the SFI correlation statistics can be observed in a given cosmology assuming the variety of observers’ characteristics to be included into the cosmic variance which is appropriate for that model.

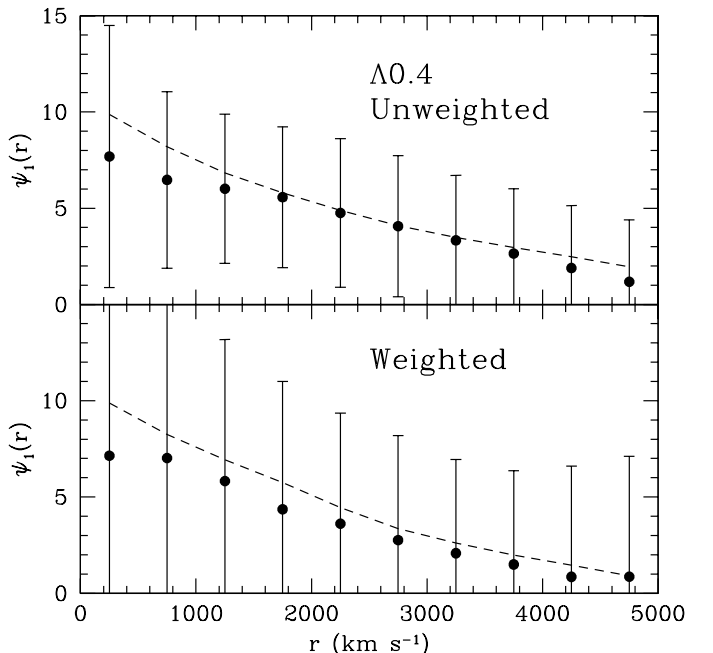


Fig. 3.— The comparison between linear-theory predictions (dashed curves) and results from the analysis of mock samples for the velocity correlation function $\psi_1(r)$ (in units of 10^4 km s^{-1}). Mock samples are extracted from an N-body simulation of the $\Lambda 0.4$ model. Upper and lower panels refer to uniform weighting and distance-error weighting, respectively. Error bars are the 1σ scatter among the set of 216 mock samples.

4.2 Testing the analysis method

Since the mock samples have been generated by reproducing the positions of real galaxies, their corresponding $\mathcal{A}(r)$ is the same as for the real SFI sample. For each cosmological model we compute in linear theory the expected ψ_1 (eq.[3]) and compare it to the distribution of values obtained from the mock samples using eq.(2). We plot in Figure 3 the results of this comparison for the $\Lambda 0.4$ case, for both uniform (upper panel) and distance–error (lower panel) weightings. Filled circles represents $\psi_1(r)$ as estimated by averaging over the set of $N_{mock} = 216$ model samples and the errorbars are the 1σ scatter, arising from both cosmic variance and observational uncertainties. As a basic result, it turns out that, for both weighting schemes, linear theory is always adequate to describe the expected velocity correlation function for samples having the same selection effects as the SFI, once they are accounted for by the $\mathcal{A}(r)$ quantity. Any residual discrepancy on small ($\lesssim 1500 \text{ km s}^{-1}$) scales, which are probably due to sampling effects or to residual non–linearities, are well within the 1σ scatter. Furthermore, we also remind that since the SFI sample only contains field spirals, we expect their dynamics to be even closer to linear theory than that of the N–body particles belonging to the mock samples, that we did not attempt to select so as to avoid high–density regions.

We checked the relative contribution to the errors from the cosmic scatter and from the uncertainties in the peculiar velocity measurements, using a set of mock samples where peculiar velocities are not perturbed according to ITF distance errors, so that only the effect of the cosmic scatter is present. It turns out that the cosmic scatter is clearly dominant at $r < 3500 \text{ km s}^{-1}$, with the TF scatter contributing $< 20\%$ and becoming relevant only at larger scales. The distance–error weighting scheme generates a larger scatter, as a consequence of the fact that this method amounts to reducing the effective volume where $\psi_1(r)$ is computed. For this reason, in the following we will take the uniform weighting as the reference analysis method to constrain model parameters.

4.3 Estimating ψ_1 uncertainties

Having demonstrated that linear theory provides reliable predictions for ψ_1 , the next information that one needs is the uncertainty to be associated to such predictions. In order to do so, we estimate from the set of mock samples the elements of the covariance matrix, \mathcal{C}^{ij} , which are defined as

$$\mathcal{C}^{ij} = \frac{1}{N_{mock}} \sum_{l=1}^{N_{mock}} (\psi_{1,l}^i - \bar{\psi}_1^i) (\psi_{1,l}^j - \bar{\psi}_1^j). \quad (6)$$

Here $\psi_{1,l}^i$ is the value of the velocity correlation function at the i –th separation bin for the l –th mock sample, while

$\bar{\psi}_1^i$ is its average value estimated over the N_{mock} samples.

Figure 4 shows the comparison between results from the $\Lambda 0.4$ and EdS models, by plotting the quantities $\mathcal{C}^{ij}/\bar{\psi}_1^i\bar{\psi}_1^j$. According to its definition, this quantity describes the relative covariance of the ψ_1 values at different separations. The top panels show the results for the diagonal (variance) terms, while the other panels show the off–diagonal terms, illustrating different rows in the covariance matrix. The first thing to note is the large cross–correlation between the results of the different bins, which are comparable to the variances, and therefore cannot be ignored when using the ψ_1 statistic to constrain cosmological models.

In addition, it is apparent from the figure that, apart from small differences due to statistical fluctuations, the two models have the same amount of relative covariance. This is not unexpected since, to a first approximation, the long–wave perturbations which generate the cosmic scatter, are also responsible for the ψ_1 signal, so as to make the relative scatter fairly constant. Noticeable differences occur only at relatively large separations, $> 3500 \text{ km s}^{-1}$, where the observational uncertainties become more dominant, thus increasing the total scatter and suppressing the discriminative power of $\psi_1(r)$. For this reason, in the following we will compare linear–theory predictions and SFI results only for $r \leq 3500 \text{ km s}^{-1}$, where the relative uncertainties are essentially the same for the two considered models. We note that, since $\Lambda 0.4$ and EdS have rather different values for both η_8 and for the power–spectrum shape, we can quite confidently conclude that the relative scatter for $\psi_1(r)$ is model–independent, at least for the range of models and scales of interest, while its absolute value is not.

In the top right panel of Fig. 4 we compare the diagonal terms for the $\Lambda 0.4$ mock samples for ψ_1 computed according to uniform and distance–error weighting schemes. It is apparent that the distance–error weighting is associated with larger error bars, as was already shown in Figure 3.

Based on these results we, therefore, conclude that: (a) the errors of individual ψ_1 bins are significantly correlated; (b) a general recipe can be devised for the ψ_1 uncertainties, whose relative amount is fairly independent of the cosmological model; and (c) that the size of such errors is smaller when ψ_1 is estimated according to the uniform–weighting scheme.

5 CONSTRAINING COSMOLOGICAL MODELS

Based on the results obtained so far, we will now use eqs.(3) and (4) as a model prediction for ψ_1 . As for the

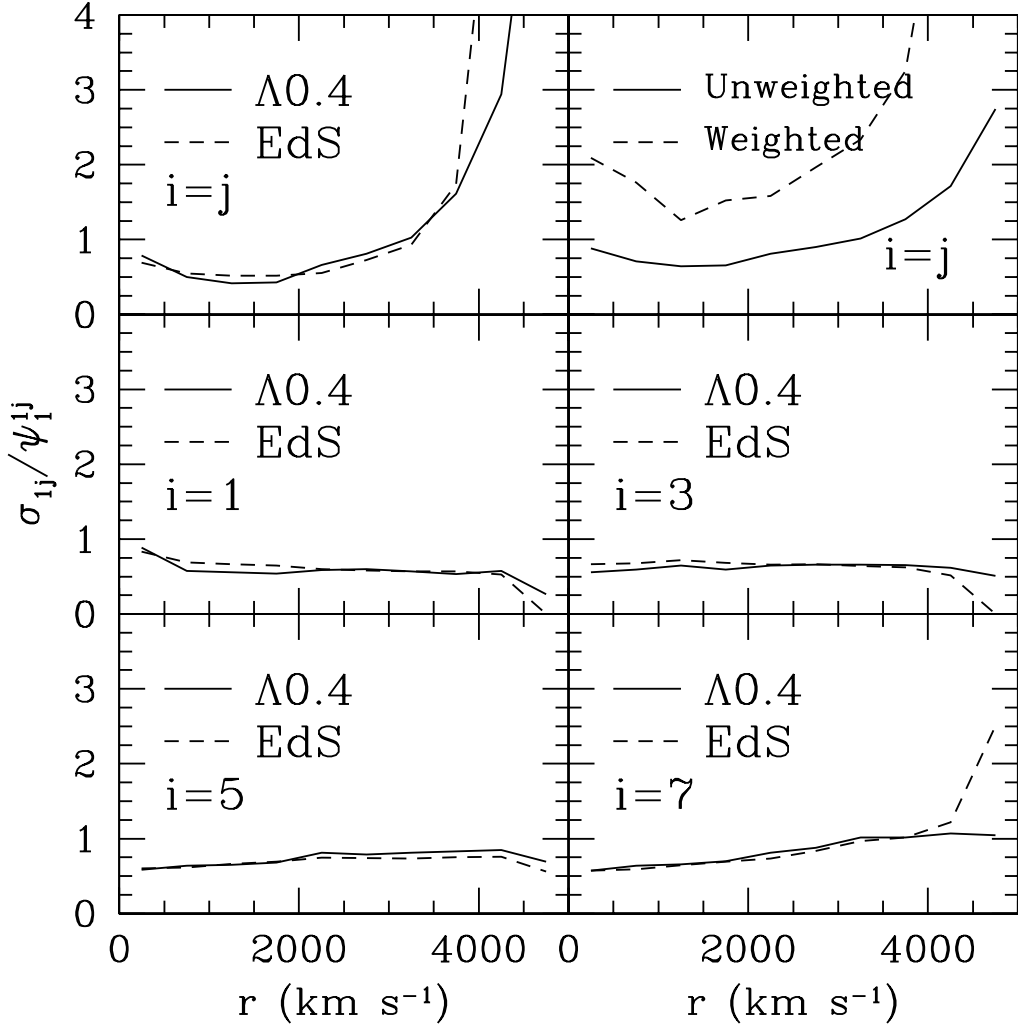


Fig. 4.— The elements of the relative covariance matrix, $C^{ij}/\psi_1^i\psi_1^j$, for SFI mock samples extracted from EdS and $\Lambda 0.4$ simulations. The top panels shows the diagonal (variance) terms, with the top right panel comparing the variance for unweighted and error-weighted estimates of $\psi_1(r)$. The other panels are for the off-diagonal terms and show different rows in the covariance matrix (see text).

model power spectrum, we express it as $P(k) = AkT^2(k)$ where we assume a Harrison-Zel'dovich shape on large scales. The transfer function, $T(k)$, is taken to be

$$T(q) = \frac{\ln(1 + 2.34q)}{2.34q} \times [1 + 3.89q + (16.1q)^2 + (5.46q)^3 + (6.71q)^4]^{-1/4} \quad (7)$$

where $q = k/\Gamma h$ and Γ is the so-called shape parameter. For $\Gamma \simeq \Omega_m h$, eq.(7) provides the transfer function for CDM models with a negligible baryon fraction (Bardeen et al. 1986). More generally, it can be seen as a phenomenological expression, with Γ a parameter to be fixed by observational constraints. As for the amplitude of the power spectrum, it is customary to express it in terms of σ_8 . Following eqs.(4), the velocity correlation function $\psi_1(r)$ is then entirely specified in linear theory by the two

parameters Γ and η_8 .

Despite the errorbars being so large such that the ψ_1 detection is only marginally different from zero in each individual bin (cf. Figs. 2 and 3), its determination at different scales does allow to place significant constraints on the η_8 - Γ plane. In order to provide constraints on these parameters, we compute the weighted χ^2 between the SFI correlation function, ψ_1^{SFI} , and that from model predictions, ψ_1^{mod} :

$$\chi^2 = \sum_{i,j} [\psi_1^{SFI}(r_i) - \psi_1^{mod}(r_i)] C_{ij}^{-1} [\psi_1^{SFI}(r_j) - \psi_1^{mod}(r_j)] \quad (8)$$

Here, C_{ij}^{-1} are the elements of the inverse of the covariance matrix, as calibrated from the mock samples, and

the sums are over the radial bins of 500 km s^{-1} width, for separations $r \leq 3500 \text{ km s}^{-1}$. The probability for model rejection is estimated by assuming a χ^2 statistic, from the value of $\Delta\chi^2 = \chi^2 - \chi_{min}^2$, where χ_{min}^2 is the absolute minimum value.

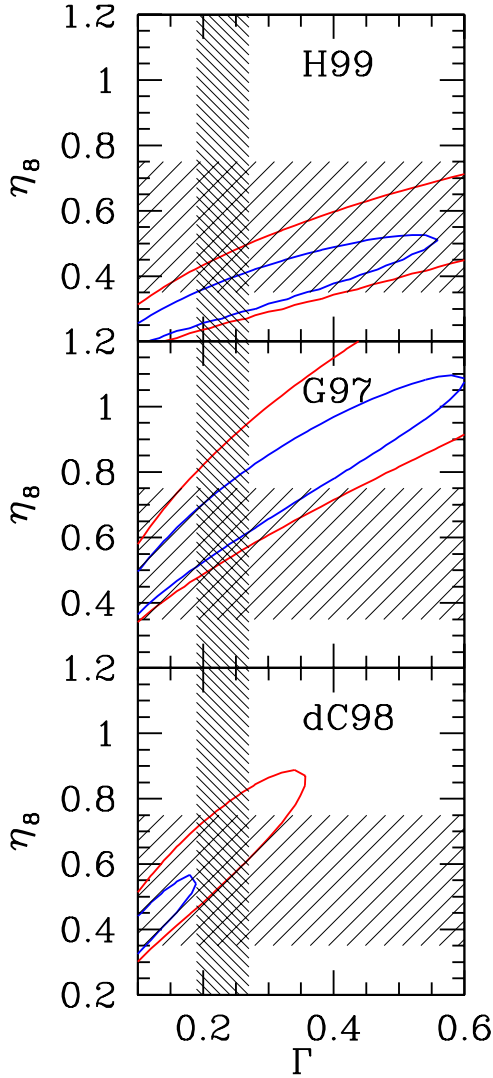


Fig. 5.— The 1σ and 2σ contours in the η_8 - Γ plane from the analysis of the velocity correlation function, $\psi_1(r)$, for different calibrations of the inverse Tully–Fisher relation. The horizontal shaded area corresponds to the 90% confidence level constraints on η_8 from the analysis of the Giovanelli et al. (1997a,b) r.m.s. cluster peculiar velocities (Borgani et al. 1997). The vertical shaded area is the 95% confidence level constraint on the shape parameter from the power–spectrum of APM galaxies (Liddle et al. 1996).

In Figure 5 we plot the iso- $\Delta\chi^2$ contours for the three ITF calibrations of the SFI sample that were discussed in Section 2. Internal and external contours correspond to $\Delta\chi^2 = 2.30$ and 6.17 , respectively, thus providing the 1σ and 2σ confidence levels for two significant parameters. The corresponding minimum values of the χ^2 per

degree of freedom are 1.67, 0.80, and 0.78, for the H99, G97 and dC98 calibrations, respectively. In all cases, the best-fitting model seems to provide an acceptable fit. This value for the H99 calibration is somewhat large, however it corresponds to only $\sim 1\sigma$ deviation for a χ^2 statistic with five degrees of freedom. The fact that such χ^2 values are around unity indicates that our error model is realistic.

The vertical shaded areas represent the 95% confidence level interval on the shape parameter, as derived by Liddle et al. (1996) from the power–spectrum of APM galaxies. The horizontal shaded areas represent the 90% confidence level on η_8 derived by Borgani et al. (1997) from an analysis of the r.m.s. peculiar velocity of SCI clusters (Giovanelli et al. 1997a). All these constraints intersect our 2σ confidence regions.

For the H99 and G97 ITF calibrations, the constraints in the η_8 - Γ plane can be cast in the form

$$\eta_8 = \eta_{8,0} \times \left(\frac{\Gamma}{0.2} \right)^{0.5}, \quad (9)$$

with $\eta_{8,0} = 0.30^{+0.12}_{-0.07}$ and $\eta_{8,0} = 0.58^{+0.22}_{-0.12}$ for the two above calibrations, respectively (errorbars correspond to 2σ c.l.). The asymmetry in the errors is due to the fact that, as η_8 is increased from its best–fitting values, larger absolute errors are assigned to ψ_1 , since the relative scatter is taken to be constant (cf. §4.3). Thus, larger values of η_8 tend to be excluded at a lower significance than smaller values. As for the dC98 calibration, the corresponding constraints show a somewhat steeper Γ -dependence of η_8 with values of $\Gamma \lesssim 0.35$ ruled out at about 2σ c.l. It is interesting to note that, for $\Gamma \simeq 0.2$, this result agrees with $\beta = 0.6 \pm 0.1$, as found by da Costa et al. (1998), for an almost unbiased IRAS galaxy distribution.

We show in Figure 6 the variation of $\Delta\chi^2$ around its minimum as a function of η_8 , in order to show the effect of changing other assumptions underlying our analysis. In all the panels, the solid curve refers to constraints from the H99 ITF calibration, for a fixed shape-parameter $\Gamma = 0.2$ and $\log W > 2.25$ for the line–width of SFI galaxies.

As demonstrated already (Fig. 2, top panel), our results are insensitive to the choice of galaxy weighting, and we adopt here throughout the uniform weighting. As is illustrated here [panel (b)], changing the limiting line–width of the sample also has a negligible effect on our results which are virtually unchanged as we increase it from 2.25 to 2.40. We find as well that our constraints do not depend on the specific choice of binning used in the computation of $\psi_1(r)$. The effect of the zero–point uncertainty is shown in panel (a). As was illustrated also in the lower panel of Figure 2, the results are quite sensitive to such changes, and a negative shift of the ITF zero–point by 0.1 mag leads to a sizeable increase of η_8 from $\simeq 0.3$ to $\simeq 0.55$. For higher values of Γ , this change would similarly corre-

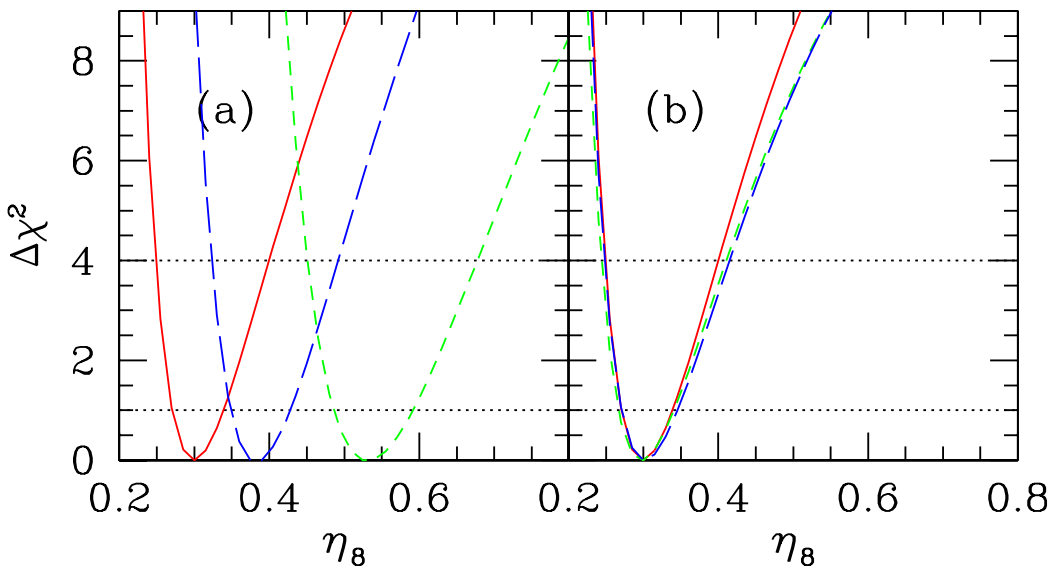


Fig. 6.— Variation of $\Delta\chi^2$ around its minimum value as a function of η_8 . In both panels the solid curve corresponds to $\Gamma = 0.2$, uniform weighting in the estimate of $\psi_1(r)$, ITF calibration by H99a,b, with the best-fitting value of the zero-point, and $\log W > 2.25$ for the galaxy line-width. Panel (a): effect of changing the zero-point of the ITF relation; short- and long-dashed lines are for shifting it by 0.1 magnitudes upwards and downwards, respectively. Panel (b): effect of increasing the limiting line-width; short- and long-dashed lines are for $\log W > 2.3$ and $\log W > 2.4$, respectively.

spond to higher values of η_8 , e.g for $\Gamma = 0.4$, η_8 would increase from $\simeq 0.4$ to $\simeq 0.8$, and its effect is generally comparable to that of varying the ITF calibration.

Despite the fact that the constraints on cosmological parameters drawn from the ψ_1 statistics are quite sensitive to the details of the ITF calibrations, some conclusions can still be drawn. First, the constraints on the velocity power-spectrum normalization, η_8 , depend on the $P(k)$ shape, as a consequence of the fact that we are probing velocity fields on scales larger than the $8h^{-1}\text{Mpc}$ normalization scale. Second, assuming $\Gamma \simeq 0.2$, as indicated by galaxy clustering data, implies power-spectrum amplitudes which can be different by up to a factor two, but are still generally consistent with independent observational constraints. For instance, the local abundance of galaxy clusters to a first approximation also provides a constraint on $\eta_8 = 0.5\text{--}0.6$ (e.g. Eke, Cole & Frenk 1996; Girardi et al. 1998, and references therein).

Our results for η_8 can also be compared with those obtained by Zaroubi et al. (1997) and FZ99, who estimated the mass power spectrum by a maximum likelihood (ML) analysis of the peculiar velocities of the Mark III and the SFI samples, respectively. These estimates are then translated to constraints on η_8 by integrating over the corresponding spectra. Both works consistently found $\eta_8 \simeq 0.8 \pm 0.2$ at 90% c.l. and a preferred value of $\Gamma \simeq 0.4 \pm 0.2$. As the application of the ML analysis for the SFI sample has been performed using the G97 calibration, it is most suitable to compare the FZ99 results with

those reported in the central panel of Fig. 5. It turns out that the confidence regions coming from the ML and ψ_1 analyses do overlap over a significant portion of the $\eta_8\text{--}\Gamma$ plane. For $\Gamma = 0.4$, the ψ_1 analysis gives $\eta_8 = 0.85^{+0.17}_{-0.10}$. The main difference being the dependence of the η_8 constraints on Γ in the ψ_1 analysis, such that for lower values of $\Gamma \simeq 0.2$ the preferred η_8 values are somewhat smaller than those obtained in the ML analysis.

One should also bear in mind the different sensitivities of these two analyses. As demonstrated in Figs. 5 and 6, the ψ_1 analysis is sensitive to the ITF calibration, while it is robust to changing the limiting line-width. On the other hand, the ML analysis is remarkably robust to changes in TF calibration (e.g. Fig. 8 in FZ99), while it is more sensitive to the pruning of SFI galaxies at different line-widths. For these reasons, these two methods should be regarded as complementary and both worth to be applied to a given data set.

6 CONCLUSION

In this paper we have presented an analysis of the velocity correlation function, $\psi_1(r)$, for the SFI sample of Sbc–Sc galaxy peculiar velocities based on the infrared TF distance indicator calibrated using a sample of cluster galaxies (Giovannelli et al. 1997a,b; Haynes et al. 1999a,b). In order to minimize uncertainties related to Malmquist bias corrections, we performed the analysis us-

ing the redshift–space positions of galaxies and the ITF distance indicator. Three different ITF calibrations for the SFI sample have been examined in our analysis: one based on an updated version of the SFI sample presented by Haynes et al. (1999a,b, H99), that presented by Giovanelli et al. (1997b, G97) and that obtained by da Costa et al. (1998, dC98).

The final goal of our analysis is to place constraints on the amplitude and the shape of the fluctuation power–spectrum, by comparing $\psi_1(r)$ from SFI and from linear–theory predictions of cosmological models. For this purpose, we needed to verify the reliability of linear–theory to predict $\psi_1(r)$ for a sample having the same galaxy positions and observational uncertainties as the SFI one, and to estimate the associated uncertainties due to cosmic scatter and observational uncertainties. These two goals have been achieved by comparing linear–theory predictions to results from the analysis of a large set of mock SFI samples, extracted from N–body simulations.

We have found that linear–theory provides a rather accurate description of the $\psi_1(r)$ estimated from the mock samples, over the whole scale range considered ($r \leq 5000 \text{ km s}^{-1}$; cf. Figure 3). This confirms that both sparse sampling effects and residual non–linearities have a minor impact on our analysis. We have also shown that the relative covariance in $\psi_1(r)$ among the set of mock samples is roughly independent of the cosmological models, thus allowing for a simple treatment of the associated errors.

In general, we find that our analysis constrains a degenerate ridge in the η_8 – Γ plane. For the H99 and G97 ITF calibrations, we find $\eta_8 = \eta_{8,0}(\Gamma/0.2)^{0.5}$, with $\eta_{8,0} = 0.30_{-0.07}^{+0.12}$ and $\eta_{8,0} = 0.58_{-0.12}^{+0.22}$ for the two above calibrations, respectively, at the 2σ level (cf. Figure 5). The dC98 exhibits a stronger tendency for lower values of the shape parameter, constraining $\Gamma \lesssim 0.35$ at the 2σ

level, and is consistent with the G97 calibration in that range. These constraints are robust to variations of the galaxy weighting scheme (cf. Figure 2) and to changes in the choice of the limiting galaxy line–width (cf. Figure 6), but are, clearly, very sensitive to uncertainties in the calibration details, such as the zero–point of the TF relation.

In any case, the results presented here indicate that the large–scale velocity field can be brought into agreement with the low fluctuation amplitude implied at $\sim 10h^{-1}\text{Mpc}$ scale by the abundance of galaxy clusters (e.g. Eke et al. 1996, Girardi et al. 1998), for power–spectrum shapes which are consistent with large–scale clustering data (e.g. Liddle et al. 1996), while higher amplitudes are allowed for larger values of the shape parameter. Our constraints on the η_8 – Γ plane for the ITF G97 calibration and those from the maximum–likelihood (ML) analysis for the G97 direct TF relation by Freudling et al. (1999, FZ99) are quite consistent for $\Gamma \gtrsim 0.3$. Since the ML and the ψ_1 methods are sensitive to different degrees to different aspects of the analysis (i.e., TF calibration and limiting line–width), they should be regarded as complementary approaches for extracting cosmological constraints from large–scale cosmic flows.

We acknowledge useful discussions with Adi Nusser, Avishai Dekel and Saleem Zaroubi. We thank the referee Michael Strauss for many useful comments, which improved the presentation of the results. We thank Hugh Couchman for the generous sharing of his adaptive P^3M code. We are grateful to the ESO Visitors fund for supporting visits to Garching by SB, RG, MPH, and IZ. SB acknowledges ICTP and SISSA in Trieste, for the hospitality during several phases of preparation of this work. IZ was supported by the DOE and the NASA grant NAG 5-7092 at Fermilab.

REFERENCES

- Aaronson, M., Huchra, J., & Mould, J.R. 1979, *ApJ*, 229, 1
 Bardeen, J.M., Bond, J.R., Kaiser, N., & Szalay A.S. 1986, 304, 15
 Borgani, S., da Costa, L.N., Freudling, W., Giovanelli, R., Haynes, M.P., Salzer, J., & Wegner, G. 1997, *ApJ*, 482, L121
 Borgani, S., Rosati, P., Tozzi, P., & Norman, C. 1999, *ApJ*, 517, 40
 Branchini E., et al. 1999, *MNRAS*, in press (astro-ph/9901366)
 Bunn, E.F., & White, M. 1997, *ApJ*, 480, 6
 Burstein, D., Davies, R.L., Dressler, A., Faber, S.M., Stone, R.P.S., Lynden–Bell, D., Terlevich, R.J., & Wegner, G.A. 1987, *ApJS*, 64, 601
 Chiu, W.A., Ostriker, J.P., & Strauss, M.A. 1998, *ApJ*, 494, 479
 Cole, S. 1997, *MNRAS*, 286, 38
 Couchman, H.M.P. 1991, *ApJ*, 368, 23
 da Costa, L.N., Freudling, W., Wegner, G., Giovanelli, R., Haynes, M.P., & Salzer, J.J. 1996, *ApJ*, 468, L5
 da Costa, L.N., Nusser, A., Freudling, W., Giovanelli, R., Haynes, M.P., Salzer, J.J., & Wegner, G. 1998, *MNRAS*, 299, 425
 Dekel, A. 1994, *Ann. Rev. Astr. Ap.*, 32, 371
 Dekel, A., Bertschinger, E., & Faber, S.M. 1990, *ApJ*, 364, 349
 Dekel, A., & Lahav, O. 1999, *ApJ*, 520, 24
 Eke, V.R., Cole, S., & Frenk C.S. 1996, *MNRAS*, 282, 263
 Ferreira, P.G., Juszkiewicz, R., Feldman, H.A., Davis, M., & Jaffe, A.H. 1999, *ApJ*, 515, L1
 Fisher, K.B., Davis, M., Strauss, M.A., Yahil, A., & Huchra, J.P. 1994, *MNRAS*, 266, 50
 Fisher, K.B., Huchra, J.P., Strauss, M.A., Davis, M., Yahil, A., & Schlegel, D. 1995, *ApJS*, 100, 69
 Freudling, W., da Costa, L.N., Wegner, G., Giovanelli, R., Haynes, M.P., & Salzer, J.J. 1995, *AJ*, 110, 920
 Freudling, W., Zehavi, I., et al. 1999, *ApJ*, 532, in press (astro-ph/9904118) [FZ99]
 Giovanelli, R., Dale, D.A., Haynes, M.P., Hardy, E., & Campusano, L.E. 1999, *ApJ*, in press (astro-ph/9906362)
 Giovanelli, R., Haynes, M.P., Herter, T., Vogt, N.P., Wegner, G., Salzer, J.J., da Costa, L.N., & Freudling W. 1997a, *AJ*, 113, 22
 Giovanelli, R., Haynes, M.P., Herter, T., Vogt, N.P., da Costa, L.N., Freudling, W., Wegner, G. & Salzer, J.J. 1997b, *AJ*, 113, 53 [G97]

- Girardi, M., Borgani, S., Giuricin, G., Mardirossian, F., & Mezzetti, M. 1998, *ApJ*, 506, 45
- Gòrski, K. 1988, *ApJ*, 332, L7
- Gòrski, K., Davis, M., Strauss, M.A., White, S.D.M., & Yahil, A. 1989, *ApJ*, 344, 1 [G89]
- Groth, E.J., Juszkiewicz, R., & Ostriker, J.H. 1989, *ApJ*, 346, 558
- Haynes, M.P., Giovanelli, R., Chamaraux, P., da Costa, L.N., Freudling, W., Salzer, J.J., & Wegner, G. 1999a, *AJ*, 117, 2039 [H99a]
- Haynes, M.P., Giovanelli, R., Salzer, J.J., Wegner, G., Freudling, W., da Costa, L.N., Herter, T., & Vogt, N.P. 1999b, 117, 1668 [H99b]
- Kaiser, N. 1988, *MNRAS*, 231, 149
- Kolatt, T., & Dekel, A. 1996, *ApJ*, 479, 592
- Liddle A.R., Lyth D.H., Schaefer R.H., Shafi Q., & Viana, P.T.P. 1996, *MNRAS*, 281, 531
- Mathewson, D.S., Ford, V.L., & Buchhorn, M. 1992, *ApJS*, 81, 413
- Monin, A.S., & Yaglom, A.M. 1975, *Statistical Fluid Mechanics* (Cambridge: MIT Press)
- Peebles, P.J.E. 1980, *The Large-Scale Structure of the Universe* (Princeton: Princeton University Press)
- Peacock, J.A., & Dodds, S.J. 1994, *MNRAS*, 267, 1020
- Sigad, Y., Dekel, A., Eldar, A., Strauss, M., & Yahil, A. 1998, *ApJ*, 495, 516
- Strauss, M.A., Cen, R.Y., & Ostriker, J.P. 1993, *ApJ*, 408, 389
- Strauss, M.A., & Willick, J.A. 1995, *Phys. Rep.*, 261, 271
- Tormen, G., & Bertschinger, E. 1996, *ApJ*, 472, 14
- Tormen, G., Moscardini, L., Lucchin, F., & Matarrese, S. 1993, *ApJ*, 411, 16 [T93]
- Watkins, R. 1997, *MNRAS*, 292, 59
- Willick, J.A., Courteau, S., Faber, S.M., Burstein, A., Dekel, A., & Strauss, M.A. 1997, *ApJS*, 109, 333
- Willick, J.A., & Strauss, M.A. 1998, *ApJ*, 507, 64
- Zaroubi, S., Zehavi, I., Dekel, A., Hoffman, Y., & Kolatt, T. 1997, *ApJ*, 486, 21
- Zehavi, I., Riess, A.G., Kirshner, R.P., & Dekel, A. 1998, *ApJ*, 503, 483
- Zel'dovich, Y.B. 1970, *A&A*, 5, 84